Chlamydomonas sp. UWO 241 Exhibits High Cyclic Electron Flow and Rewired Metabolism under High Salinity^{1[OPEN]}

Isha Kalra,^a Xin Wang,^a Marina Cvetkovska,^b Jooyeon Jeong,^c William McHargue,^c Ru Zhang,^c Norman Hüner,^d Joshua S. Yuan,^e and Rachael Morgan-Kiss^{a,2,3}

^aDepartment of Microbiology, Miami University, Oxford, Ohio 45056

ORCID IDs: 0000-0002-6185-9893 (I.K.); 0000-0002-7174-3042 (X.W.); 0000-0001-8723-6961 (N.H.); 0000-0003-4783-5358 (R.M.-K.)

The Antarctic green alga *Chlamydomonas* sp. UWO 241 (UWO 241) is adapted to permanent low temperatures, hypersalinity, and extreme shade. One of the most striking phenotypes of UWO 241 is an altered PSI organization and constitutive PSI cyclic electron flow (CEF). To date, little attention has been paid to CEF during long-term stress acclimation, and the consequences of sustained CEF in UWO 241 are not known. In this study, we combined photobiology, proteomics, and metabolomics to understand the underlying role of sustained CEF in high-salinity stress acclimation. High salt-grown UWO 241 exhibited increased thylakoid proton motive flux and an increased capacity for nonphotochemical quenching. Under high salt, a significant proportion of the upregulated enzymes were associated with the Calvin-Benson-Bassham cycle, carbon storage metabolism, and protein translation. Two key enzymes of the shikimate pathway, 3-deoxy-D-arabinoheptulosonate 7-phosphate synthase and chorismate synthase, were also up-regulated, as well as indole-3-glycerol phosphate synthase, an enzyme involved in the biosynthesis of L-Trp and indole acetic acid. In addition, several compatible solutes (glycerol, Pro, and Suc) accumulated to high levels in high salt-grown UWO 241 cultures. We suggest that UWO 241 maintains constitutively high CEF through the associated PSI-cytochrome b_6 supercomplex to support robust growth and strong photosynthetic capacity under a constant growth regime of low temperatures and high salinity.

During photosynthesis, light is transduced into stored energy through two major pathways, linear electron

[OPEN] Articles can be viewed without a subscription. www.plantphysiol.org/cgi/doi/10.1104/pp.19.01280

flow (LEF) and cyclic electron flow (CEF). In addition to satisfying the ATP shortage for efficient carbon fixation (Kramer and Evans, 2011), CEF-generated ATP may be used for other energy-requiring processes, such as the CO₂-concentrating mechanism of C₄ photosynthesis (Takabayashi et al., 2005; Ishikawa et al., 2016), N₂ fixation in cyanobacteria heterocysts (Magnuson et al., 2011; Magnuson and Cardona, 2016), and survival under environmental stress (Suorsa, 2015). In addition, CEF is utilized under short-term stress by rapidly inducing a transthylakoid pH change and triggering nonphotochemical energy dissipation (Lucker and Kramer, 2013; Yamori et al., 2016). Previously, it was assumed that CEF was dependent upon state transitions (Iwai et al., 2010); however, recent studies suggest that CEF induction is independent of state transitions and is sensitive to other signals (Takahashi et al., 2013; Strand et al., 2015).

The formation of protein supercomplexes has been associated with CEF initiation (Minagawa, 2016; Nawrocki et al., 2019). The first supercomplex was isolated by Iwai et al. (2010) in *Chlamydomonas reinhardtii* under dark/anaerobiosis. The supercomplex is composed of PSI, light-harvesting complex II (LHCII), cytochrome $b_6 f$ (cyt $b_6 f$), PGR5-like1 protein, and ferredoxin NADP

^bDepartment of Biology, University of Ottawa, Ottawa K1N 6N5, Ontario, Canada

^cDonald Danforth Plant Science Center, St. Louis, Missouri 63132

^dDepartment of Biology and Biotron Centre for Experimental Climate Change, University of Western Ontario, London N6A 3K7, Ontario, Canada

^eDepartment of Plant Pathology and Microbiology, Texas A&M University, College Station, Texas 77840

¹This work was supported by the National Science Foundation (grant no. 1637708 to R.M.-K. and I.K.), the U.S. Department of Energy (grant no. DE-SC0019138 to R.M.-K., I.K., and X.W. and grant no. DE-SC0019464 to J.J., W.M., and R.Z.), and the Donald Danforth Plant Science Center startup fund (to R.Z.).

²Senior author.

 $^{^3\}mbox{Author}$ for contact: morganr2@miamioh.edu.

The author responsible for distribution of materials integral to the findings presented in this article in accordance with the policy described in the Instructions for Authors (www.plantphysiol.org) is: Rachael Morgan-Kiss (morganr2@miamioh.edu).

I.K. and R.M.-K. conceived of and designed the experiments; R.M.-K. supervised the experiments; I.K. performed growth physiology, fluorescence, and Suc density gradient experiments; X.W. and J.S.Y. performed and analyzed proteome experiments; J.J. and I.K. performed the in vivo spectroscopy measurements using IDEAspec; J.J. analyzed the IDEAspec data; W.M. optimized the spectroscopy measurements using IDEAspec; R.Z. supervised and designed the spectroscopy measurements using IDEAspec; M.C. and N.H. performed and analyzed metabolome experiments; I.K. and R.M.-K. wrote the article with contributions of all the authors.

reductase (Iwai et al., 2010). Terashima et al. (2012) identified another supercomplex in *C. reinhardtii* that is formed under conditions of anoxia and is regulated through the calcium-sensing protein, CAS. Recently, the structure of the *C. reinhardtii* PSI supercomplex was solved, which showed that dissociation of specific LHCI proteins (Lhca2 and Lhca9) is necessary prior to PSI supercomplex formation (Steinbeck et al., 2018).

Around the globe, there are communities of photosynthetic organisms that have adapted to capture light energy and fix carbon under environmental conditions that are untenable for most model plant and algal species, including permanent low-temperature environments in the Arctic and Antarctic (Morgan-Kiss et al., 2006; Dolhi et al., 2013). The McMurdo Dry Valleys form the largest polar desert on the Antarctic continent and harbor numerous permanently ice-covered lakes (Priscu et al., 1999; Morgan-Kiss et al., 2006). Microalgal communities residing in the McMurdo lakes are adapted to extreme conditions, including low temperatures, nutrient deficiency, supersaturated oxygen levels, and hypersalinity (Morgan-Kiss et al., 2006).

Chlamydomonas sp. UWO 241 (UWO 241) was isolated from Lake Bonney in the 1990s (Neale and Priscu, 1990, 1995). In its native environment, UWO 241 is exposed to year-round low temperatures (0°C-5°C), hypersalinity (700 mm NaCl), and extreme shade ($\stackrel{<}{\sim}$ 20 μ mol photons m⁻² s⁻¹), with available light of a narrow spectral range (350-450 nm). In early studies, it was reported that UWO 241 appeared to exhibit permanent down-regulation of PSI, estimated by a weak P700 photooxidation and an absence of a discernible PSI chlorophyll a low-temperature (77K) fluorescence emission peak under a range of treatments (Morgan-Kiss et al., 2002a, 2005; Szyszka et al., 2007; Cook et al., 2019). Morgan-Kiss et al. (2002b) reported that UWO 241 lacks phosphorylation of LHCII and state transitions. Recently, Szyszka-Mroz et al. (2019) showed that UWO 241 exhibits some LHCII phosphorylation and cold-adapted forms of the thylakoid protein kinases Stt7 and Stl1. They suggested that UWO 241 may rely on energy spillover between PSII and PSI rather than state transitions (Szyszka-Mroz et al., 2019).

UWO 241 maintains sustained CEF under steadystate growth conditions that is associated with a PSIcyt $b_6 f$ supercomplex (Szyszka-Mroz et al., 2015; Cook et al., 2019). The formation of the UWO 241 PSI-cyt $b_6 f$ supercomplex is present only in cultures acclimated to high salinity (700 mm NaCl), and its stability is disrupted in the presence of the kinase inhibitor, staurosporine (Szyszka-Mroz et al., 2015). These previous studies suggest a role for sustained CEF activity in UWO 241 to survive long-term exposure to high salinity; however, the specific benefits of this are not understood. Here, we investigated whether the outcomes of CEF provide UWO 241 with constitutive photoprotection ability or energy generation (i.e. ATP synthesis). We hypothesized that CEF-associated alterations in energy production would be associated with downstream changes in carbon metabolism. Therefore, in addition to CEF measurements, we conducted comparative whole-cell proteomics and metabolomics to understand the effect of these CEF-associated changes on downstream metabolism of UWO 241. Our results indicate that CEF under long-term acclimation to high salinity is associated with the rewiring of primary carbon metabolism.

RESULTS

UWO 241 Is Adapted to Low Temperature and High Salt

UWO 241 was isolated from the deep photic zone (17-m sampling depth) of the hypersaline, perennially ice-covered Lake Bonney (McMurdo Dry Valleys, Victoria Land; Neale and Priscu, 1990, 1995). As a consequence of more than two decades of study, this photopsychrophile has emerged as a model for photosynthetic adaptation to permanent low temperatures (Morgan-Kiss et al., 2006; Dolhi et al., 2013; Cvetkovska et al., 2017). In addition to psychrophily, UWO 241 exhibits robust growth and photosynthetic performance under high salt (0.7 M NaCl; Supplemental Fig. S1; Morgan et al., 1998; Pocock et al., 2011).

UWO 241 Possesses Constitutively High Rates of CEF

PSI activity was monitored by far-red (FR) light-inducible P700 photooxidation (Fig. 1). Following a rise in A_{820} , reflecting FR light-induced P700 oxidation, we compared rates of P700 rereduction in the dark in

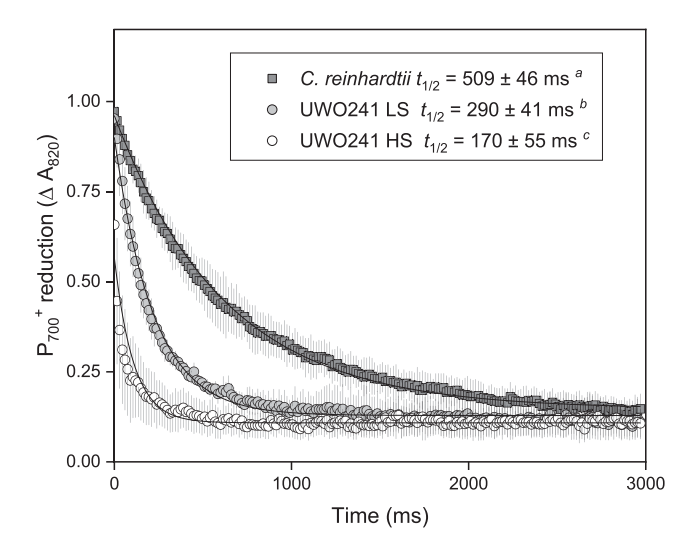


Figure 1. P700 rereduction kinetics of PSI in UWO 241 compared with the model mesophile *C. reinhardtii*. *C. reinhardtii* was grown in LS Bold's Basal Medium (BBM) at 20° C/100 μ mol m⁻² s⁻¹. UWO 241 was grown in either BBM (LS) or BBM + 700 mM NaCl (HS) and 8° C/50 μ mol m⁻² s⁻¹. t_{1/2}, Half-time for P700 rereduction. Data are means \pm so (n = 6–9). Values labeled with different lowercase letters indicate statistical differences (Student's t test, unequal variance; P < 0.05).

low-salt (LS) cultures of *C. reinhardtii* as well as LS- and high-salt (HS)-grown cells of UWO 241 (Fig. 1). Since FR light preferentially excites PSI and not PSII, reduction of P700 following FR light exposure is mainly due to alternative electron donors (Ivanov et al., 1998). UWO 241 grown in standard LS growth medium exhibited a significantly shorter rereduction time for P700⁺ $(t_{1/2}^{\text{red}})$ compared with LS-grown *C. reinhardtii* (P < 0.05; Fig. 1). Moreover, HS-grown UWO 241exhibited a 1.71-fold faster $t_{1/2}^{\text{red}}$ compared with LSgrown cultures (P < 0.05; 170 ± 55 versus 290 ± 41 ms, respectively; Fig. 1). The P700 absorbance kinetics also revealed that the oxidation of P700 in UWO 241 was less complete in HS conditions (Supplemental Fig. S2). These data indicate that relative to the model C. reinhardtii, UWO 241 exhibits a high capacity for PSIdriven CEF, which is further enhanced during acclimation to long-term high-salinity stress.

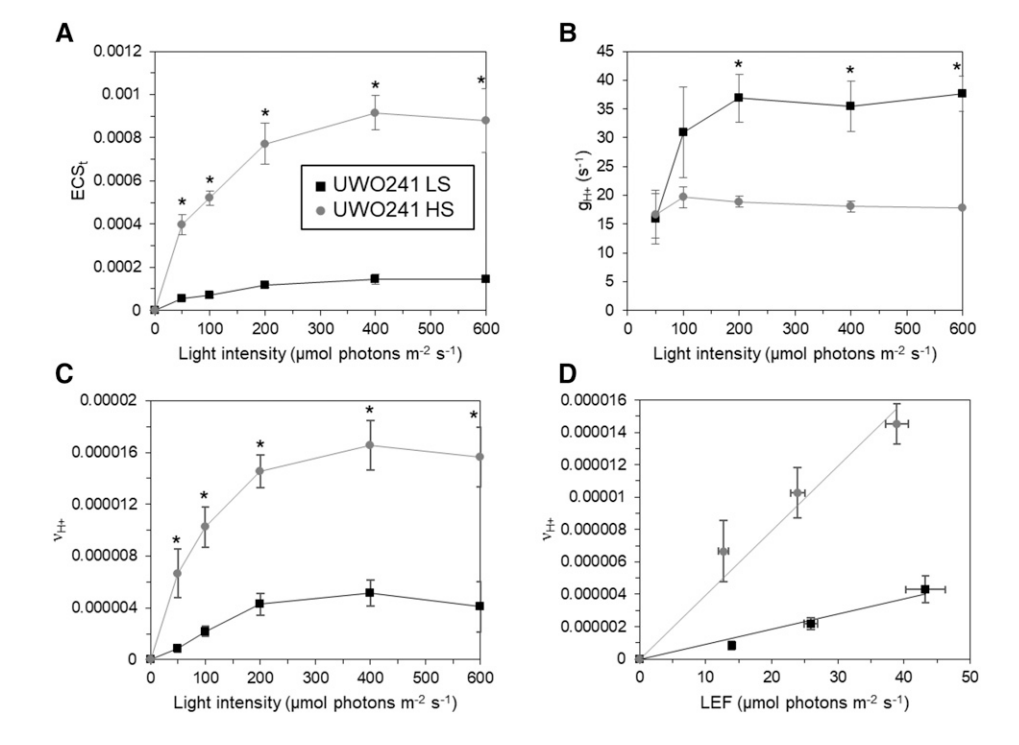
Higher rates of CEF in UWO 241-HS were also confirmed by electrochromic shift (ECS) kinetics, which estimate transthylakoid proton flux driven by lightdependent photosynthesis (Fig. 2; Supplemental Fig. S3). The ECS signal was measured by the change in absorbance of thylakoid pigments at 520 nm during the application of light-dark interval kinetics (Baker et al., 2007). The total amplitude of ECS signal (ECS_t) was used to estimate the total proton motive force (pmf) across thylakoid membranes (Kramer et al., 2003). UWO 241 grown in HS exhibited 6- to 7.5-fold higher ECS_t than that of LS-grown cells under all light intensities (Fig. 2A), suggesting that HS-grown cells generate higher pmf than LS-grown cells at the same light intensity. To verify which process(es) contributed to high pmf in HS-grown cells, proton conductance

 (g_{H+}) and fluxes through ATP synthase (ν_{H+}) were analyzed (Kanazawa and Kramer, 2002; Livingston et al., 2010; Carrillo et al., 2016). The inverse of the lifetime of the rapid decay of ECS $(1/\tau_{ECS})$ represents the proton permeability or conductivity (g_{H+}) of the thylakoid membrane and is largely dependent on the activity of ATP synthase (Supplemental Fig. S3D; Baker et al., 2007). The g_{H+} of HS-grown cells was \sim 50% to 60% compared with that of LS-grown cells (Fig. 2B); however, the ν_{H^+} showed that the amount of ATP produced was still higher in HS-grown cells (Fig. 2C). The relationship between ν_{H+} and LEF can be used to estimate proton contribution from CEF (Baker et al., 2007). In the linear plots of ν_{H+} versus LEF, the slope of the HS-grown cells was higher than that of LS-grown cells (Fig. 2D), indicating that CEF contributes significantly to the $\nu_{\rm H+}$ in HS-grown cells. Thus, in close agreement with our P700 findings, UWO 241-HS exhibited higher rates of CEF compared with UWO 241-LS (Figs. 1 and 2D). Lastly, HS-grown cells exhibited increased capacity for nonphotochemical quenching (NPQ; Supplemental Fig. S3, A and B), while PSI photochemical yield was higher in HS- versus LS-grown (P = 0.07) cells due to reduced PSI acceptor side limitation (Supplemental Fig. S4).

Isolation of a PSI Supercomplex in UWO 241

The formation of PSI supercomplexes has been shown to be essential for the induction of CEF in plants and algae (DalCorso et al., 2008; Iwai et al., 2010). An earlier report showed that high salinity-acclimated cultures of UWO 241 form a PSI supercomplex (UWO

Figure 2. Photosynthetic properties of UWO 241 under various light intensities using ECS. A to C, The ECS_t (proportional to pmf; A), gH+ (reflecting ATP synthase activity; B), and ν_{H^+} (reflecting proton flux through ATP synthase; C) of UWO 241 grown in LS (black squares) and HS (gray circles) conditions were measured from dark interval relaxation kinetics. D, The relationship between ν_{H+} and LEF (measured by chlorophyll fluorescence; Supplemental Fig. S2) was assessed in UWO 241. Data are means \pm sD (n = 3). Asterisks indicate statistical differences (Student's t test, unequal variance; *P < 0.05).



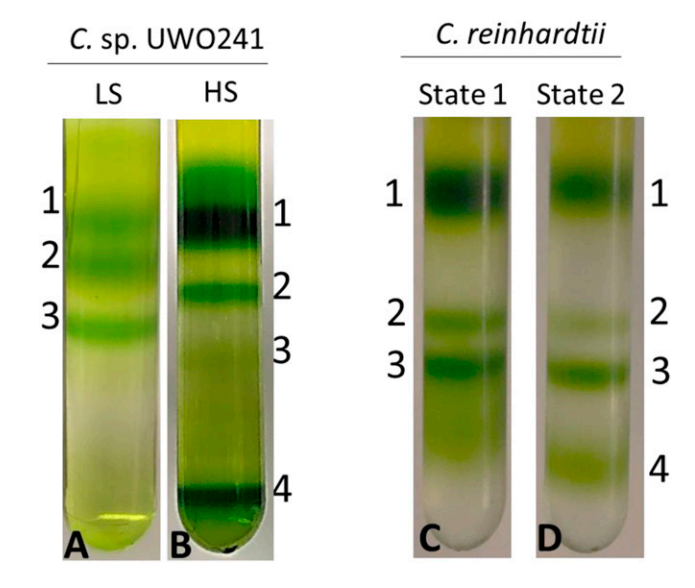


Figure 3. Supercomplex formation in UWO 241 versus *C. reinhardtii*. A and B, Fractionation of major thylakoid chlorophyll-protein complexes from UWO 241 by Suc density ultracentrifugation from LS- and HS-grown cultures (A and B, respectively). C and D, Fractionation of major thylakoid chlorophyll-protein complexes from *C. reinhardtii* exposed to state 1 and state 2 conditions (C and D, respectively). Cultures of *C. reinhardtii* were grown under control conditions (20°C/100 μ mol m⁻² s⁻¹) and either dark adapted for 10 min (state 1; C) or incubated under anaerobic conditions for 30 min (state 2; D). Band 1, LHCII; band 2, PSII core; band 3, PSI-LHCI; band 4, supercomplex.

241-SC); however, the yield of the UWO 241-SC from fractionated thylakoids was relatively low and only a few proteins were identified (Szyszka-Mroz et al., 2015). In agreement with this report, the Suc gradient from thylakoids isolated from UWO 241-LS had three distinct bands corresponding to major LHCII (band 1), PSII core complex (band 2), and PSI-LHCI (band 3; Fig. 3A). In contrast, UWO 241-HS thylakoids lacked a distinct PSI-LHCI band but exhibited several heavier bands, including the UWO 241-SC band (band 4; Fig. 3B). We significantly improved recovery of the UWO 241-SC by solubilizing thylakoids with the detergent *n*-dodecyl- α -maltoside (α -DDM) rather than β -DDM, which was used by other groups (Fig. 3B). As a control, we compared the banding pattern of C. reinhardtii thylakoids when cells were exposed to the treatment typically used by others to induce supercomplex formation (i.e. state 1 versus state 2 conditions; Iwai et al., 2010; Takahashi et al., 2013; Fig. 3, C and D, respectively). In contrast with UWO 241, band 3 (PSI) was more prominent while the supercomplex band (band 4) was diffuse in state 2-treated C. reinhardtii cells (Fig. 3D).

Low-temperature fluorescence spectra were analyzed for the four bands extracted from the Suc density gradients shown in Figure 3, B and D (i.e. UWO 241-HS and state 2-treated *C. reinhardtii*, respectively). In *C. reinhardtii*, band 1 exhibited a major emission peak at 680 nm (Fig. 4A, corresponding to fluorescence from

LHCII; Krause and Weis, 1991). Band 2 exhibited an emission peak at 685 nm, consistent with the PSII core (Fig. 4A). Band 3 exhibited a peak at 685 nm and a strong peak at 715 nm; the latter was consistent with PSI-LHCI (Fig. 4A). However, band 4 exhibited a strong fluorescence peak at 680 nm and a minor peak at 715 nm (Fig. 4A).

Fractionated thylakoids from UWO 241-HS exhibited emission spectra for band 1 and band 2 that were comparable with that from *C. reinhardtii* (Fig. 4B). In contrast, both band 3 and band 4 (PSI and supercomplex bands, respectively) exhibited highly reduced

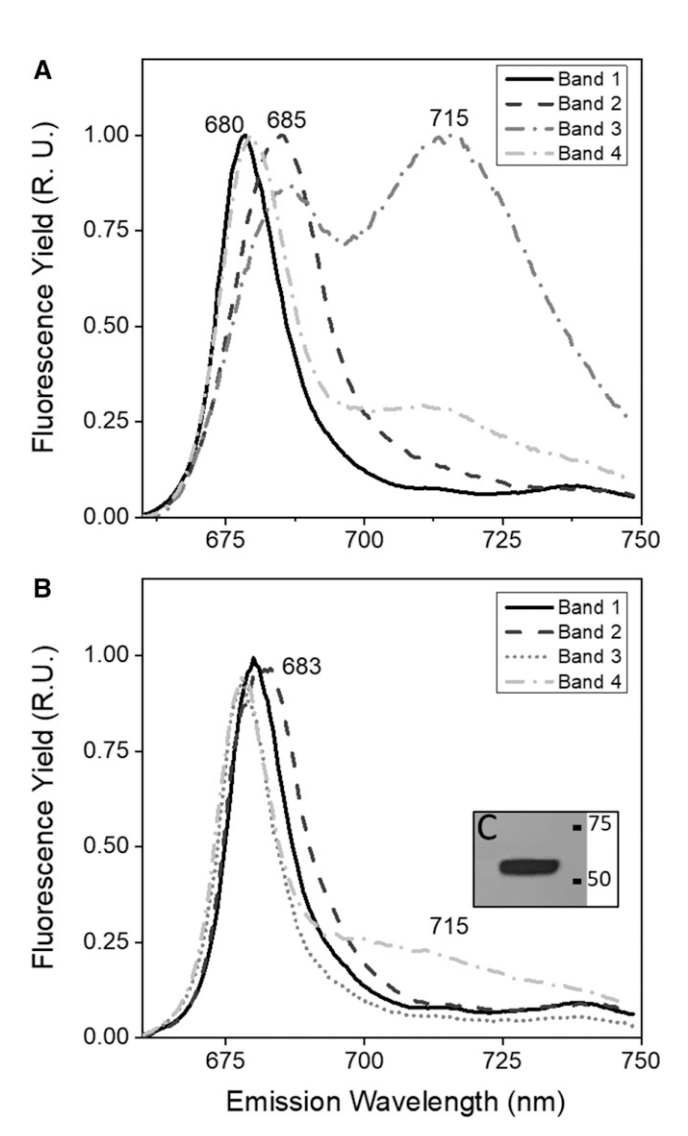


Figure 4. 77K fluorescence emission spectra of chlorophyll-protein complexes from *C. reinhardtii* and UWO 241. Low-temperature chlorophyll *a* fluorescence emission spectra are shown for pigment-protein bands isolated from Suc density gradients shown in Figure 3. A, Low-temperature chlorophyll *a* emission spectra of bands from *C. reinhardtii* state II conditions. B, Emission spectra of bands from HS cultures of UWO 241. C, Immunoblot of the UWO 241-SC band with PsaA anti-body. Spectra represent normalized data and the average of three scans. R.U., Relative unit.

or a lack of fluorescence associated with PSI. However, we confirmed the presence of the PSI reaction center protein, PsaA, in the UWO 241-SC by immunoblotting (Fig. 4C).

Protein Composition of the Supercomplex

Protein components of the UWO 241-SC were analyzed using liquid chromatography-tandem mass spectrometry (LC-MS/MS). We identified a total of 39 proteins in the isolated band 4. The most abundant proteins in the supercomplex were proteins of the PSI reaction center and cyt $b_6 f$. In total, we identified seven of 13 subunits of the PSI reaction center (Table 1; Supplemental Table S1). Only two LHCI subunits, Lhca3 and Lhca5, and one LHCII minor subunit, CP29, were associated with the UWO 241-SC. CAS was identified as the fourth most abundant protein in the UWO 241-SC. We also identified four subunits of ATP synthase in the UWO 241-SC (α , β , γ , and δ). Previously identified FtsH and PsbP proteins were also detected.

Bands 3 and 4 contained many PSI core proteins but lacked almost all Lhca proteins (Supplemental Table S1). To determine whether the absence of Lhcas in the UWO 241 proteome was due to a loss of *Lhca* genes, we searched a UWO 241 transcriptome generated from a culture grown under low temperature/high salinity (Raymond et al., 2009). We identified nine *Lhca* homologs that were transcribed under high salinity, suggesting that all or most of the *Lhca* genes are expressed in UWO 241 (Supplemental Fig. S5).

Whole-Cell Proteome Analysis

We wondered whether constitutively high CEF could be linked to changes in downstream metabolism in UWO 241. To address this question, whole-cell proteomes extracted from cultures of UWO 241-LS and UWO 241-HS under optimal temperature/light conditions were compared. Overall, 98 proteins from various functional categories were identified as significantly affected in the two treatments, out of which 55 were up-regulated and 43 were down-regulated in HS-acclimated cells. Proteins associated with photosynthesis (19%), translational machinery (19%), and other metabolism (18%) were most affected in the treatment. This was followed by proteins belonging to the carbohydrate and storage metabolism (11%) category (Supplemental Fig. S6).

Table 1. The UWO 241 supercomplex contains subunits of PSI, cyt b₆f, ATP synthase, as well as several antenna proteins

Proteomic analysis is shown for band 4 isolated from cultures acclimated to high salinity (700 mm NaCl; Fig 3B). Percentage NSAF (normalized spectral abundance factor) values for selected proteins are shown. The identity of the organism with the protein of the closest homology is also reported.

Protein	Percentage NSAF	UniProtKB	Organism
PSI			
PsaD	4.53	Q39615	C. reinhardtii
PsaE	4.24	P12356	C. reinhardtii
PsaF	3.12	P12356	C. reinhardtii
PsaH	1.84	P13352	C. reinhardtii
PsaK	6.13	P14225	C. reinhardtii
PsaL	2.43	Q39654	Cucumis sativus
LHCI and LHCII antenna			
Lhca3	1.35	Q9SY97	Arabidopsis
Lhca5	2.82	Q9C639	Arabidopsis
CP29	2.25	Q93WD2	C. reinhardtii
LHCII type I	2.22	P20866	Physcomitrella patens
CB2	9.46	P14273	C. reinhardtii
Cyt b ₆ f			
PetA	5.35	P23577	C. reinhardtii
PetB	2.33	Q00471	C. reinhardtii
PetC	1.15	P49728	C. reinhardtii
ATP synthase			
ATP synthase α	2.45	P26526	C. reinhardtii
ATP synthase β	2.07	P06541	C. reinhardtii
ATP synthase δ	1.15	P26360	Ipomoea batatas
ATP synthase γ	1.12	Q96252	Arabidopsis
Other			
CAS	4.65	Q9FN48	Arabidopsis
FtsH1	0.49	Q5Z974	Oryza sativa
FtsH2	1.26	O80860	Arabidopsis
PsbP	2.52	P11471	C. reinhardtii

Photosynthesis

Differentially regulated proteins participating in photosynthesis were identified in UWO 241-HS. Three photosystem reaction center proteins, PsaB and PsaN of PSI and D2 of PSII, as well as extrinsic proteins of the water-oxidizing complex, PsbO and PsbQ, were downregulated in UWO 241-HS (Figs. 5 and 6A; Supplemental Table S2). One protein of chloroplastic ATP synthase, the ε -subunit, was up-regulated (3.8-fold) in UWO 241-HS. Last, both FtsH proteins that were detected in the UWO 241-SC, FtsH1 and FtsH2, were up-regulated in UWO 241-HS (Table 1; Supplemental Table S3).

Several proteins associated with the Calvin-Benson-Bassham (CBB) cycle were significantly up-regulated in UWO 241-HS cells (Figs. 5 and 6A; Supplemental Table S3). The Rubisco large subunit was up-regulated in UWO 241-HS, along with two chaperone proteins involved in Rubisco assembly, RuBA and RuBB. A class

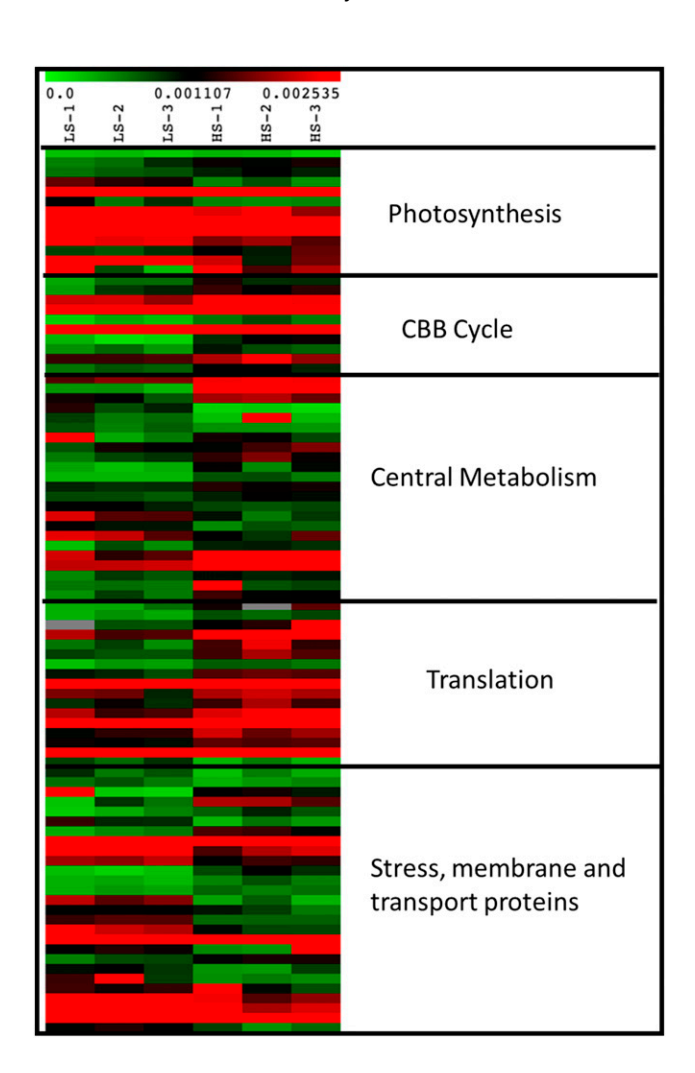


Figure 5. Heat map of differentially regulated proteins in UWO 241 under LS and HS conditions. The normalized spectral abundance factor values are plotted for each replicate in the two conditions (n = 3) using a color-based approach (green, low abundance; red, high abundance). The proteins are categorized into broad processes to which they belong.

2 Fru-1,6-bisphosphatase (FBPase) was the third highest up-regulated protein (5-fold), and Fru bisphosphate aldolase and transketolase were also up-regulated in UWO 241-HS (Fig. 6; Supplemental Table S3).

Metabolism

The enzyme glycerol-3-phosphate dehydrogenase, involved in glycerol biosynthesis, was the highest upregulated enzyme in UWO 241-HS cultures (6-fold; Fig. 6B; Supplemental Table S3). Fru bisphosphate aldolase, involved in gluconeogenesis and feeding into starch synthesis, as well as Glc-1-P adenylyltransferase (AGPase) and starch synthase1 (the last enzyme in the starch synthesis pathway) were also up-regulated in UWO 241-HS (Fig. 6B; Supplemental Table S3).

Two key enzymes from the shikimate pathway were significantly up-regulated in UWO 241-HS: (1) the first enzyme in the pathway, DAHP (3-deoxy-D-arabinoheptulosonate 7-phosphate) synthase (2.3-fold), and (2) the last enzyme in the pathway, chorismate synthase (1.9-fold; Fig. 6B; Supplemental Table S3). Indole-3-glycerol phosphate synthase was also up-regulated significantly in the HS conditions.

Primary Metabolome Analysis

We detected a total of 771 unique metabolic signatures, 179 of which were positively identified based on their mass spectra and retention times (Supplemental Table S4; Kind et al., 2009). A heat map of all measured (identified and unidentified) metabolites showing the relative changes in primary metabolite abundances indicated clustering and a discrete population of metabolites that accumulate at high levels in HS-grown cultures when compared with LS-grown cells (Supplemental Fig. S7). Overall, 59 metabolites (32%) were significantly different (false discovery rate-adjusted P < 0.05), out of which nine were present in higher abundance and 50 were present in lower abundance in HS- versus LS-grown UWO 241 cultures (Supplemental Tables S5 and S6).

We observed high levels of glycerol in the primary metabolome of HS-grown UWO 241 (8.7 FC) and high accumulation of the compatible solutes Suc (18.2 FC) and Pro (27.1 FC; Supplemental Table S5). We also observed a high accumulation of phytol (12.6 FC), suggesting chlorophyll degradation. UWO 241-HS cultures exhibited decreased amounts of 17 amino acids and compounds associated with amino acid metabolism (Supplemental Table S6). Most notable metabolites from this class were Lys (29.4 FC) and Orn (14 FC), which could signify a shift in amino acid metabolism to Pro during exposure to high salinities. We also observed lower levels of the amino acid Trp (2.8 FC) in HS-grown cultures. Metabolites involved in purine and pyrimidine metabolism were present in lower amounts in UWO 241 exposed to high salinity, suggesting that these cells have shifted their metabolism from maintenance of

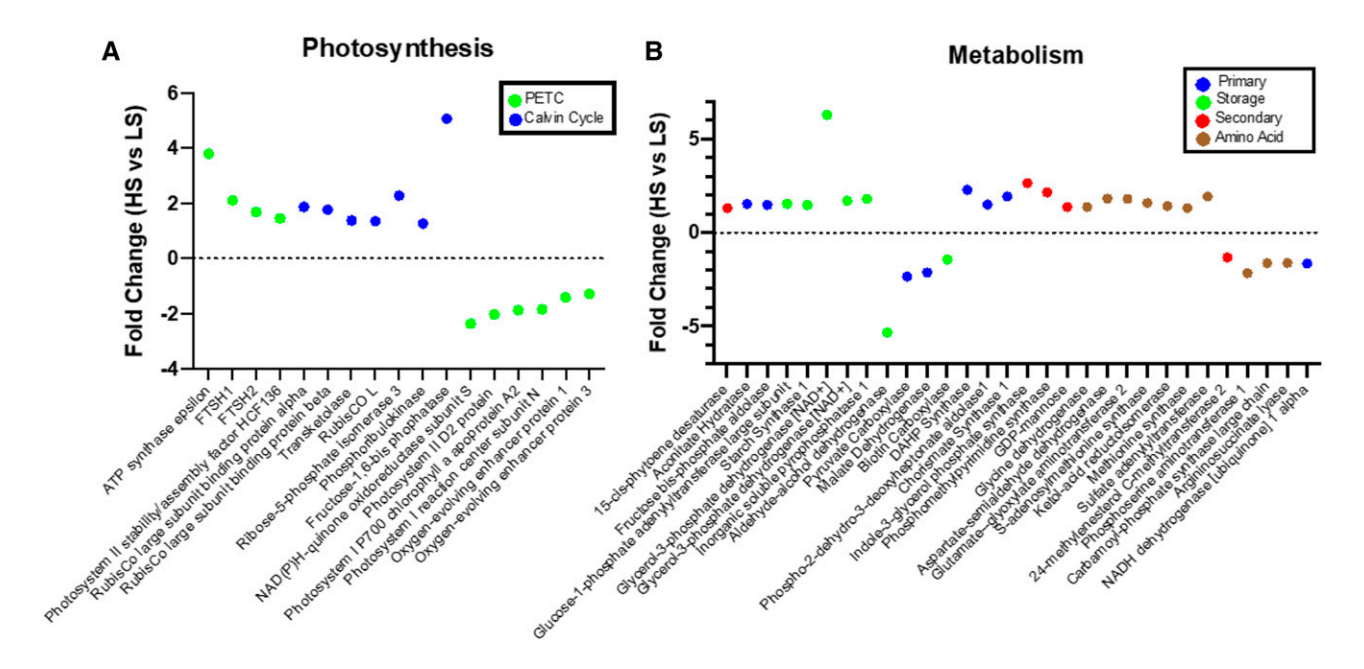


Figure 6. Changes in photosynthetic machinery and downstream metabolism in UWO 241 associated with high salinity. A, Proteins participating in photosynthetic machinery (photosynthetic electron transport chain [PETC], green; Calvin cycle, blue) significantly affected in UWO 241 under high salinity. B, Proteins participating in downstream metabolism that belong to primary (blue), storage (green), secondary (red), and amino acid biosynthesis (brown) metabolic pathways significantly affected in UWO 241 under high salinity. Proteins with fold change (FC) > 1.2 are shown (n = 3).

the cell cycle and nucleic acid synthesis to producing osmoprotectants and compatible solutes. We also observed a reduction of 3-phosphoglycerate (2.9 FC) in HS-grown cultures.

DISCUSSION

Our study shows that UWO 241 maintains robust growth and photosynthesis under the combined stress of low temperature and high salt. This ability differs markedly from other model plants and algae that typically display down-regulation of photosynthesis and growth when exposed to environmental stress, mainly as a consequence of bottlenecks in carbon fixation capacity (Hüner et al., 1998, 2003, 2016; Ensminger et al., 2006). Previous research has thoroughly described adaptive strategies for survival under permanent low temperatures, while survival under hypersalinity has received less consideration (Morgan et al., 1998; Morgan-Kiss et al., 2002a; Szyszka et al., 2007; Possmayer et al., 2011).

One of the more distinct photosynthetic characteristics of UWO 241 is the presence of a strong capacity for PSI-driven CEF (Morgan-Kiss et al., 2002b; Szyszka-Mroz et al., 2015; Cook et al., 2019). We validated that CEF rates are high in HS-grown cultures using the ECS signal, which was purported to mitigate problems with using P700 absorbance changes for CEF estimates (Lucker and Kramer, 2013). While CEF appears to be essential in plants and algae for balancing the ATP/NADPH ratio

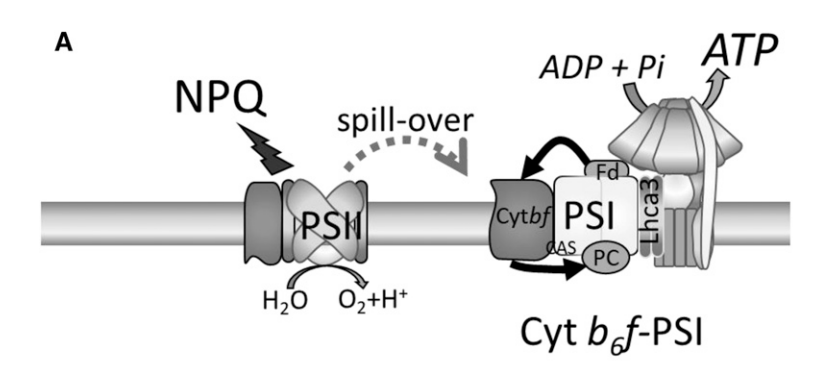
and protecting both PSI and PSII from photooxidative damage (Munekage et al., 2004; Joliot and Johnson, 2011; Huang et al., 2012), most studies report that CEF is part of short-term stress acclimation. Our work here, as well as other studies, suggest a larger role for CEF during long-term adaptation under permanent environmental stress (Morgan-Kiss et al., 2002b; Szyszka-Mroz et al., 2015; Cook et al., 2019).

Constitutively high rates of CEF in UWO 241 are associated with a general reorganization of PSI and PSII complexes (Szyszka-Mroz et al., 2019) and the formation of a PSI-cyt $b_6 f$ supercomplex (Szyszka-Mroz et al., 2015). In this study, following optimization of thylakoid protein complex solubilization by substituting β -DDM with α -DDM, the vast majority of PSI shifted from free PSI in the LS-grown cultures to association with the UWO 241-SC in the HS-grown cultures. PSI supercomplexes have been described in several plant and algal species (Iwai et al., 2010; Li et al., 2018; Steinbeck et al., 2018). The UWO 241-SC is distinct from that of C. reinhardtii because (1) its assembly is independent of short-term exposure to dark anaerobic conditions or other state transition-inducing treatments (Fig. 3), (2) the vast majority of PSI in UWO 241 is associated with the UWO 241-SC (Fig. 3), and (3) isolated UWO 241-SC and PSI bands as well as whole cells lack typical PSI fluorescence emission at 77K, despite the presence of several PSI core proteins (Fig. 4; Table 1; Supplemental Table S1; Morgan et al., 1998; Morgan-Kiss et al., 2002a, 2002b; Cook et al., 2019). Thus, CEF combined with significant structural and functional

changes to PSI are major targets for long-term stress acclimation in UWO 241 (Fig. 7A).

While the UWO 241-SC contains most of the PSI core proteins, both the UWO 241-SC and PSI bands, as well as whole-cell proteomes isolated from LS and HS conditions, lacked homologs for most LHCI proteins (Table 1; Supplemental Table S1). This agrees with an earlier study that was unable to detect most of the LHCI polypeptides by immunoblotting in UWO 241 thylakoids (Morgan et al., 1998). Cook et al. (2019) also reported that the absence of LHCI proteins in UWO 241 was not associated with adaptation to chronic iron deficiency, an additional stress experienced by natural communities of this alga. Transcriptomic analyses detected nine Lhca homologs in UWO 241 grown under low temperature/high salinity (Supplemental Fig. S5). Therefore, it appears that while most of the *Lhca* genes are encoded for and transcribed, few of the LHCI proteins are produced under the growth conditions tested thus far. These results fit well with numerous unsuccessful attempts to elicit typical 77K PSI long-wavelength fluorescence emission in UWO 241 (Morgan et al., 1998; Morgan-Kiss et al., 2002a, 2002b, 2005; Szyszka et al., 2007; Cook et al., 2019). It also explains the differences in the 77K emission spectra of the UWO 241-SC and PSI bands between UWO 241 and *C. reinhardtii* (Fig. 4). Lastly, a recent study reported that UWO 241 transfers light energy from PSII to PSI via constitutive energy spillover through an undescribed mechanism (Szyszka-Mroz et al., 2019). Thus, UWO 241 favors down-regulated LHCI and constitutive energy spillover in response to its extreme habitat, most likely the natural light environment of extreme shade enriched in blue wavelengths (Neale and Priscu, 1995).

The direct product of CEF is extra transthylakoid pmf at the expense of NADPH production (Lucker and Kramer, 2013; Dumas et al., 2016; Yamori et al., 2016), with the consequence of CEF impacting either cellular energy production or photoprotection. CEF-dependent formation of a pH gradient protects PSII by activating energy-dependent quenching, a major process for dissipation of excess light energy in PSII (Yamori et al., 2016). Alternatively, CEF-generated pmf can be used for the production of additional ATP for high-energy-consuming processes, including protein synthesis, transport processes, ion homeostasis (He et al., 2015), CO₂-concentrating mechanisms (Horváth et al., 2000;



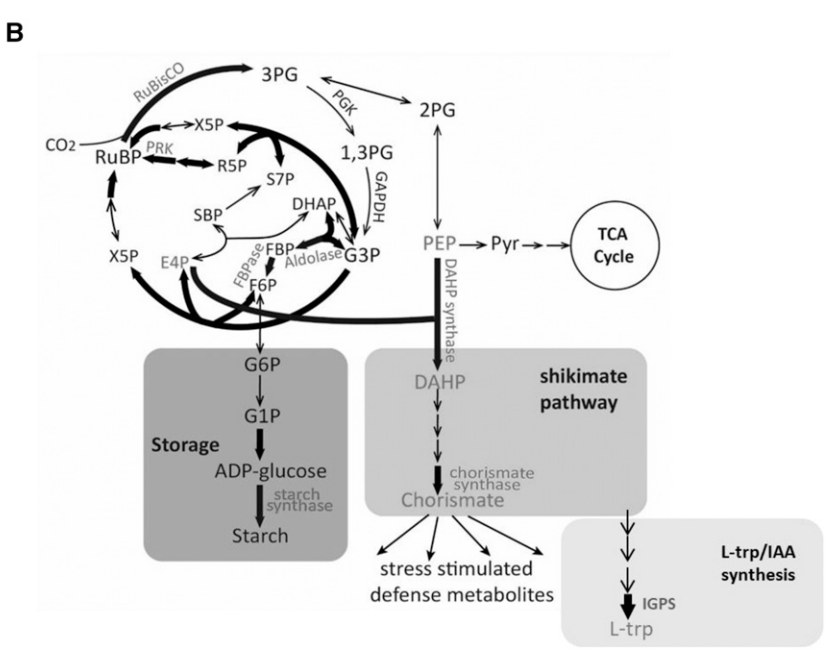


Figure 7. A restructured photosynthetic apparatus supports the rewiring of central metabolism in UWO 241. A, The photosynthetic apparatus of UWO 241 is assembled to promote high rates of CEF sustained by the formation of a PSI-cyt $b_6 f$ supercomplex. CEF supports the photoprotection of PSII and PSI and provides additional ATP for downstream metabolism. B, ATP is consumed, in part, by the CBB cycle as well as an up-regulated shikimate pathway and carbon storage pathways (starch, glycerol). The model is based on data presented here and in other studies (Szyszka-Mroz et al., 2015, 2019; Cook et al., 2019). Fd, Ferredoxin; IAA, indole acetic acid; PEP, phosphoenolpyruvate; Pyr, pyrimidine; RuBP, ribulose-1,5-bisphosphate; TCA, trichloroacetic acid.

Lucker and Kramer, 2013), or production of secondary metabolites (Murthy et al., 2014). Lastly, CEF prevents PSI photoinhibition by down-regulating LEF and alleviating overreduction of the acceptor side of PSI, thereby preventing reactive oxygen-induced PSI damage (Munekage et al., 2008; Shimakawa et al., 2016; Chaux et al., 2017; Huang et al., 2017). A strong constitutive CEF mechanism in UWO 241 could be beneficial for one or most of the above purposes. First, HS-grown cultures possess a higher capacity for NPQ (Supplemental Fig. S3), supporting a role for CEF in constitutive photoprotection ability. High CEF rates also match up with a higher PSI photochemical yield and a lower PSI acceptor side limitation in HS-grown cultures (Supplemental Fig. S4), suggesting enhanced PSI photoprotection in UWO 241-HS cells.

UWO 241-HS cells exhibited significantly higher levels of cellular ATP compared with UWO 241-LS cells (Supplemental Fig. S8). In addition, ATP synthase subunits were associated with the UWO 241-SC (Table 1), suggesting that CEF contributes extra ATP in UWO 241. HS-grown cultures exhibited significantly higher ECS_t and ν_{H+} compared with LS-grown cultures, suggesting a high flux of protons through the chloroplastic ATP synthase in spite of slow activity of ATP synthase (compare Fig. 2, A and C, with Fig. 2B). Slower activity of ATP synthase could be overcome by higher abundance of ATP synthase subunits in the UWO 241-HS, which is reported here (Figs. 5 and 6) and in an earlier report (Morgan et al., 1998). Recently, it was shown that in a salt-tolerant soybean (*Glycine max*), increased CEF contributes to excess ATP that is used to drive the import of Na⁺ in the vacuole (He et al., 2015). Taken together, constitutively high rates of CEF in UWO 241 are likely to provide dual benefits, that of constitutive photoprotection of both PSI and PSII and extra ATP to support downstream processes important for low-temperature and/or high-salinity adaptation (Fig. 7A).

Comparison of whole-cell proteomes and metabolomes revealed significant shifts in primary metabolism in LS- and HS-grown UWO 241. First, HS-grown cultures have a strong carbon fixation potential. Key enzymes within the CBB cycle are up-regulated under HS, including large subunit of Rubisco (EC 4.1.39) and a chaperone complex involved in Rubisco assembly (RuBA and RuBB proteins). Several enzymes important in regeneration of ribulose-1,5-bisphosphate, including FBPase (EC 3.1.3.11), Fru bisphosphate aldolase (EC 4.1.2.13), transketolase (EC 2.2.1.1), ribose-5 phosphate isomerase (EC 5.2.1.6), and phosphoribulokinase (EC 2.7.1.19), are also more abundant in HS-grown cells (Fig. 7B). Overexpression of key bottleneck CBB enzymes such as FBPase and SBPase enhances carbon fixation and ribulose-1,5-bisphosphate regeneration (Lefebvre et al., 2005; Tamoi et al., 2006) while also supporting improved photosynthesis during stress (Driever et al., 2017). Low levels of 3-phosphoglycerate, the direct by-product of Rubisco activity, also suggest strong carbon sinks for fixed CO₂ in HS-grown cultures (Supplemental Table S6). Lastly, overproduction of these key CBB enzymes is supported by a robust protein translation ability, as several ribosomal proteins are also overexpressed in HS-grown cells (Supplemental Table S3).

Enhanced CBB pathway activity would support robust photosynthetic activity and growth in UWO 241. However, proteomic evidence revealed other potential carbon sinks, including carbon storage in the form of starch (Supplemental Table S3). Two key enzymes of starch synthesis were up-regulated under high salinity, AGPase (EC 2.7.7.27) and starch synthase (EC 2.4.1.242). AGPase catalyzes the formation of Glc-1-P to ADP-Glc and consumes one ATP. ADP-Glc serves as a substrate for starch synthase to extend the glucosyl chain in starch. In contrast with these findings, plant and algal fitness and survival under low temperatures or high salinity are associated with starch degradation (for review, see Thalmann et al., 2016). Under abiotic stress, starch is remobilized into sugars and other metabolites to provide carbon and energy when photosynthesis is compromised. In contrast with cold- or salt-sensitive plants and algae, the photosynthetic apparatus of UWO 241 is remodeled to support photosynthesis under continuous low temperatures and high salinity (Morgan et al., 1998; Szyszka et al., 2007; Pocock et al., 2011). Thus, the accumulation of starch in UWO 241 may act as a strong carbon sink to support high rates of carbon fixation (Fig. 7B). Starch stored in the chloroplast is also transitory and is often rapidly turned over (Thalmann et al., 2016). Starch content was comparable between LS- and HS-grown UWO 241 cultures (Supplemental Fig. S9). Thus, transiently stored starch could be an additional adaptive strategy in UWO 241, acting as an energy and carbon buffer that can be rapidly mobilized when needed. This theory is supported by other publications that reported accumulation of starch under cold or salinity stress (Siaut et al., 2011; Wang et al., 2013), suggesting that transitory starch synthesis and mobilization may be important during stress acclimation.

The shikimate pathway is an essential link between primary and secondary metabolism for producing precursors for aromatic amino acids (Trp, Phe, and Tyr) as well as many other aromatic metabolites (Maeda and Dudareva, 2012). It is a high-carbon-flux pathway, accounting for approximately 30% of all fixed CO_2 in an organism (Tohge et al., 2013). Various biotic and abiotic stresses up-regulate genes of the shikimate pathway as well as downstream biosynthesis pathways that use the main product of the shikimate pathway, chorismate, as a substrate (Tzin and Galili, 2010). UWO 241-HS exhibited up-regulation of two key shikimate enzymes, DAHP synthase (EC 2.5.1.54) and chorismate synthase (EC 4.2.3.5). The substrates for DAHP synthase are erythrose-4-phosphate (E4P) and 2-phospho*enol*pyruvate. E4P is a product of the CBB cycle enzyme transketolase. Up-regulation of transketolase in HS-grown cells indicates that E4P would be supplied in high levels to support high flux

through the shikimate pathway. On the other hand, the supply of 2-phospho*enol*pyruvate for chorismate synthesis is likely to come from glycolysis, as indicated by the higher level of expression of glycerol-3-phosphate dehydrogenase under the HS condition (Supplemental Table S3). Thus, the CBB cycle and glycolysis are likely to be coordinated to provide substrates to support high flux through the shikimate pathway. Lastly, there is evidence linking CEF with the shikimate pathway. One recent study involving a CEF mutant of Arabidopsis (*Arabidopsis thaliana*) lacking PGR5 protein showed that the levels of shikimate metabolites were significantly reduced in the CEF mutant as compared with the wild type, suggesting a link between CEF and chorismate synthesis (Florez-Sarasa et al., 2016).

Despite more than two decades of study on UWO 241, there are many questions that remain unanswered regarding how this enigmatic organism thrives in an environment inhospitable to most of life on Earth. Recent articles have added to the breadth of knowledge on the photosynthetic apparatus, including a cold-adapted ferredoxin isoform (Cvetkovska et al., 2018) and a thylakoid kinase exhibiting temperature-dependent phosphorylation patterns (Szyszka-Mroz et al., 2019). Here, we extend our understanding of long-term photosynthetic adaptation to permanent cold and hypersalinity by proposing a model for sustained PSI-CEF that supports a robust growth and photosynthesis (Fig. 7). Under permanent environmental stress, CEF supplies constitutive photoprotection of PSI and PSII while also producing extra ATP for downstream metabolism (Fig. 7A). The restructured photosynthetic apparatus is accompanied by a major rewiring of central metabolism to provide a strong carbon fixation potential that is used in part to produce stored carbon and drive high-carbon-flux pathways (Fig. 7B). Algae adapted to multiple stressors, such as low temperatures combined with high salinity, are robust fixers of CO₂, providing new genetic targets for improving crop stress resistance and previously unconsidered sources of natural carbon sinks.

MATERIALS AND METHODS

Culture Conditions and Growth Physiology

Chlamydomonas sp. UWO 241 (CCMP1619) was grown in either BBM (0.43 mm NaCl; LS) or BBM supplemented with 700 mm NaCl (HS). Based on earlier studies (Morgan et al., 1998), UWO 241 cultures were grown under a temperature/irradiance regime of 8° C/50 photons μ mol m⁻² s⁻¹. Chlamydomonas reinhardtii UTEX 90 was grown in BBM (LS) at 20°C/100 μmol photons m⁻² s⁻¹. All cultures were grown in 250-mL glass Pyrex tubes in temperatureregulated aquaria under a 24-h light cycle and were continuously aerated with sterile air supplied by aquarium pumps (Morgan-Kiss et al., 2008). Growth was monitored daily by optical density at a wavelength of 750 nm. Maximum growth rates were calculated using natural log transformation of the optical density values during the exponential phase. Three biological replicates were performed, and all subsequent experiments were conducted on log phase cultures. Oxygen evolution was measured at 8°C with Chlorolab 2 (Hansatech) based on a Clark-type oxygen electrode, following the method described by Jeong et al. (2017). Cellular ATP and starch were determined using commercial kits, an ATP colorimetric/fluorometric assay kit (catalog no. K354; BioVision) and a starch assay kit (catalog no. SA20; Sigma-Aldrich), respectively. For

supercomplex isolation, C. reinhardtii cells were exposed to either state 1 or state 2 conditions. For state 1 induction, midlog phase cells were incubated in darkness for 10 min to completely oxidize the plastoquinone pool. For state 2 induction, midlog phase cells were incubated in the dark under anaerobic conditions (N_2 bubbling) for 30 min.

Low-Temperature (77K) Fluorescence Spectra

Low-temperature chlorophyll *a* fluorescence emission spectra of whole cells and isolated chlorophyll-protein complexes were measured using Luminescence Spectrometer LS50B (Perkin-Elmer) as described by Morgan-Kiss et al. (2008) at 436 nm and 5-nm (isolate complexes) or 8-nm (whole cells) slit width. Prior to the measurement, cultures were dark adapted for 10 min. Decompositional analysis was performed using a nonlinear least-squares algorithm using Microcal OriginPro Version 8.5.1 (Microcal Origin). The fitting parameters for the Gaussian components (position, area, and full width half-maximum) were free-running parameters.

P700 Oxidation-Reduction and CEF

FR light-induced photooxidation of P700 was used to determine rates of CEF as described by Morgan-Kiss et al. (2002b). A volume of exponential phase cultures representing 25 μg of chlorophyll a was dark adapted for 10 min and then filtered onto 25-mm GF/C filters (Whatman). Filters were measured on the Dual-PAM 100 instrument using the leaf attachment. The proportion of photooxidizable P700 was determined by monitoring absorbance changes at 820 nm and expressed as the parameter $\Delta A_{820}/A_{820}$. The signal was balanced and the measuring light switched on. FR light ($\lambda_{\rm max}=715$ nm, 10 W m $^{-2}$; Scott filter RG 715) was then switched on to oxidize P700. After steady-state oxidation levels were reached, the FR light was switched off to rereduce P700. The $t_{1/2}^{\rm red}$ was calculated after the FR light was turned off as an estimate of relative rates of PSI-driven CEF (Ivanov et al., 1998). The rereduction time for P700 was calculated using Microcal Origin software (Microcal Software).

In Vivo Spectroscopy Measurements

Saturation-pulse chlorophyll fluorescence yield changes and dark interval relaxation kinetics of the ECS were measured at 8°C with the IDEA spectrophotometer as described previously with some modifications (Sacksteder and Kramer, 2000; Zhang et al., 2009). First, 2.5 mL of cells supplemented with 25 μ L of 0.5 M NaHCO₃ was preincubated in the dark for 10 min and followed by 10 min of illumination of FR light. The chlorophyll fluorescence and ECS were measured with the cells acclimated for 5 min in various actinic light intensities provided by red light-emitting diodes. The PSII operating efficiency (Φ_{PSII}) was calculated as $F_q{'}/F_m{'}$ and NPQ as $(F_m-F_m{'})/F_m{'}$. The LEF was calculated from the following equation: LEF = $A \times (fraction_{PSII}) \times I \times \Phi_{PSII}$, where I is the light intensity, A is the absorptivity of the sample, which is generally assumed to be 0.84, and fraction_{PSII} is the fraction of absorbed light stimulating PSII (Baker, 2008). The fraction_{PSII} values of UWO 241 grown in LS and HS, measured by 77K fluorescence spectra, were 0.709 and 0.746, respectively. The ECS_t was used to estimate the pmf. The g_{H+} was estimated from the inverse of the lifetime of the rapid decay of ECS (Baker et al., 2007). All ECS signals were normalized to the rapid rise in ECS induced by a single turnover flash to account for changes in pigmentation (Livingston et al., 2010).

Thylakoid Isolation

Thylakoids were isolated according to Morgan et al. (1998). Midlog phase cultures were collected by centrifugation at 2,500g for 5 min at 4°C. All buffers were kept ice-cold and contained 1 mm Pefabloc Sc (Sigma) and 20 mm NaF. The pellet was resuspended in grinding buffer (0.3 m sorbitol, 10 mm NaCl, 5 mm MgCl₂, 5 mm MgCl₂, 1 mm benzamidine, and 1 mm aminocaproic acid). The cells were disrupted using a chilled French press at 10,000 pounds per square inch twice and then centrifuged at 23,700g for 30 min. The thylakoid pellet was resuspended in wash buffer (50 mm Tricine-NaOH [pH 7.8], 10 mm NaCl, and 5 mm MgCl₂) and centrifuged at 13,300g for 20 min. The pellet was resuspended in storage buffer (0.3 m sorbitol, 10% [v/v] glycerol, 50 mm Tricine-NaOH [pH 7.8], 10 mm NaCl, and 5 mm MgCl₂) and stored at $-80^{\circ}\mathrm{C}$ until analysis.

SDS-PAGE and Immunoblotting

SDS-PAGE was performed using the Bio-Rad Mini-Protean system and a 12% urea-SDS gel (Laemmli, 1970). Thylakoid membranes were denatured using 50 mM DTT and incubated at 70°C for 5 min. Samples were loaded on an equal protein basis (10 $\mu {\rm g}$ of total protein). Proteins were transferred to a nitrocellulose membrane using cold-wet transfer at 100 V for 2.5 h. The membrane was blocked with Tris-buffered saline + Tween with 5% (w/v) milk (Carnation). A primary antibody against PsaA (catalog no. AS06-172; Agrisera) was used at a 1:1,000 dilution to probe for the major reaction center protein of PSI. Membranes were then exposed to Protein A conjugated to horseradish peroxidase, and blots were detected with ECL Select Western Blotting Detection Reagent (Amersham).

Supercomplex Isolation

Suc step density centrifugation was used to isolate supercomplexes from exponentially grown cultures according to Szyszka-Mroz et al. (2015) with some modifications. Every step was performed in darkness and on ice. All buffers contained phosphatase (20 mm NaF) and protease (1 mm Pefabloc Sc) inhibitor. Cells were collected by centrifugation, and the pellet was washed twice in buffer 1 (0.3 \upmu Suc, 25 mm HEPES-KOH [pH 7.5], and 1 mm MgCl2). Cells were disrupted using a French press as described above, and broken cells were spun down at 50,000g for 30 min. The pellet was resuspended in buffer 2 (0.3 M Suc, 5 mм HEPES-KOH [pH 7.5], and 10 mм EDTA) and centrifuged at 50,000g for 30 min. The thylakoid pellet was resuspended gently in buffer 3 (1.8 m Suc, 5 mm HEPES-KOH [pH 7.5], and 10 mm EDTA) and transferred to an Ultra-clear tube (catalog no. 344060; Beckman Coulter). The thylakoid prep was overlaid with buffer 4 (1.3 m Suc, 5 mm HEPES-KOH [pH 7.5], and 10 mm EDTA) followed by buffer 5 (0.5 M Suc and 5 mm HEPES-KOH [pH 7.5]). This Suc step gradient was ultracentrifuged at 288,000g for 1 h at 4°C using an SW40Ti rotor (Beckman Coulter). Purified thylakoids were collected and diluted (threefold) in buffer 6 (5 mm HEPES-KOH [pH 7.5] and 10 mm EDTA) and centrifuged at 50,000g to pellet the membrane. Linear Suc gradients were made using the freeze-thaw method with buffer 7a (1.3 \pm Suc, 5 mM HEPES-KOH [pH 7.5], and 0.05% [w/v] α -DDM) and buffer 7b (0.1 m Suc, 5 mm HEPES-KOH [pH 7.5], and 0.05% [w/v] α -DDM). Briefly, two dilutions of buffers 7a and 7b were made, buffer 7-1 (2× buffer 7a + 1× buffer 7b) and buffer 7-2 (1× buffer 7a + 2× buffer 7b). To make the gradient, first, 3 mL of buffer 7a was poured into 12-mL Ultra-clear tubes followed by flash freezing in liquid nitrogen. Next, buffer 7-1 was poured on top, followed by flash freezing. This was repeated for buffer 7-2 and buffer 7b, respectively. The frozen gradients were kept at 4°C overnight to thaw. For supercomplex isolation, thylakoid membranes (0.4 mg of chlorophyll) were resuspended in 1% (w/v) α -DDM (catalog no. D99020; Glycon Biochemicals) and incubated on ice in the dark for 25 min. Membranes were spun down to remove insoluble material and loaded onto the linear Suc gradient described above (0.1–1.3 M Suc) containing 0.05% (w/v) α -DDM. Gradients were centrifuged at 288,000g for 21 h at 4°C using an SW40Ti rotor (Beckman Coulter). Protein complexes were extracted using a 21-gauge needle.

Sample Preparation for Proteomics

Whole-cell proteins were extracted as described previously (Valledor and Weckwerth, 2014). Midlog phase cells were collected by centrifugation at 2,500g for 5 min (50 mg wet weight). The cell pellets were resuspended in an extraction buffer containing 100 mм Tris-HCl (pH 8), 10% (v/v) glycerol, 2 mм Pefabloc Sc, 10 mм DTT, and 1.2% (v/v) plant protease inhibitor cocktail (catalog no. P9599; Sigma). Samples were transferred to 2-mL screw-cap tubes containing 25 mg of zirconia beads (catalog no. A6758; Bio-Rad) and homogenized three times for 45 s in a BeadBeater (BioSpec). Then, 20% (w/v) SDS solution was added to the tubes, and samples were incubated for 5 min at 95°C. The denatured proteins were centrifuged at 12,000g to pellet any insoluble material. Protein pellets were resuspended in 1.5 mL of Tris buffer (50 mm Tris-HCl, pH 8) containing 0.02% $(w/v)\beta$ -DDM (Glycon Biochemicals) and supplemented with 1× Halt protease and phosphatase inhibitor cocktail (Thermo-Scientific). After the protein extraction, the sample preparation for proteomics was conducted following our previously published method (Wang et al., 2016). Specifically, 100 μg of total protein was treated with 8 m urea/5 mm DTT for 1 h at 37°C, followed by alkylation with 15 mm iodoacetamide in the dark for 30 min at room temperature. Samples were then diluted fourfold with 50 mm Tris-HCl buffer and digested using mass spectrometry-grade Trypsin Gold (Promega) at 1:100 (w/w)

concentration for 16.5 h at 37°C. The digested samples were cleaned using Sep-Pak C18 plus desalting columns (Waters).

Proteomic Analyses by LC-MS/MS

The whole-cell proteomics were conducted using Multidimensional Protein Identification Technology-based shotgun proteomics by loading digested peptides onto a biphasic strong cation-exchange/reverse-phase capillary column. Two-dimensional LC-MS/MS was conducted on an LTQ ion-trap mass spectrometer (Thermo Finnegan) operated in the data-dependent acquisition mode. The full mass spectra were recorded at 300 to 1,700 mass-to-charge ratio, and the five most abundant peaks of each scan were selected for MS/MS analysis. The MS/MS raw data were analyzed by first converting into MS2 files, followed by database search using ProLuCID (Xu et al., 2006). The UWO 241 protein database was generated based on our transcriptomics data supplemented with 37 common contaminants and their reversed sequences as a quality-control system to restrain false-positive discovery to 0.05. Differentially expressed proteins were analyzed using PatternLab for Proteomics (Carvalho et al., 2008). The proteomics results have been deposited to the MassIVE repository with the identifier MSV000084382.

For identifying protein components in the supercomplex, the complex was harvested and 30 μg of total protein was processed similarly as described above to get the digested peptides. Different from the whole-cell proteomics, the processed peptides were directly loaded onto a capillary C18 column without fractionation and further analyzed in a Thermo LTQ Orbitrap XL mass spectrometer. The full mass spectra were recorded in the range of 350 to 1,800 mass-to-charge ratio with a resolution of 30,000. The top 12 peaks of each scan were selected for MS/MS analysis. The data analysis was conducted similarly as described above.

Homologs of Lhca proteins were identified from a transcriptome previously generated from UWO 241 (Raymond et al., 2009; National Center for Biotechnology Information BioProject no. PRJNA575885).

Gas Chromatography-Mass Spectrometry

For determination of the primary metabolome, UWO 241 was grown in four biological replicate cultures as described above. Algal cells were harvested by centrifugation (6,000g, 5 min, 4°C) and washed once with fresh medium. The supernatant was decanted, and the algal cells were flash frozen in liquid nitrogen and stored at -80°C. Metabolite extractions and gas chromatographymass spectrometry measurements were performed at the West Coast Metabolomics Center (University of California, Davis) following protocols from Fiehn et al. (2008). Mass spectra were processed using BinBase, an application system for deconvoluting and annotating mass spectral data, and analyzed at the West Coast Metabolomics Center as described (Fiehn et al., 2005). Metabolites were identified based on their mass spectral characteristics and gas chromatography retention times, by comparison with compounds in a plant and algae reference library. Peak heights for the quantification ion at the specific retention index corresponding to each metabolite were normalized by the sum of peak heights in the sample. Data processing, normalization, and statistical analysis were performed in-house. Normalized data were processed by cube root transformation followed by range scaling (van den Berg et al., 2006). Statistical analyses were performed by the Metaboanalyst 4.0 software suite (Chong et al., 2018) and included principal component analysis, Student's t test, heat map, and clustering analysis using Ward's linkage for clustering and Pearson's correlation as a measure of dissimilarity.

Accession Numbers

Sequence data reported in this article can be found in the GenBank database under the accession number PRJNA575885 for *Lhca* genes. The accession numbers of proteins from band 3 in Supplemental Table S1 are as follows: PsaB (P36492), PsaD (Q39615), PsaE (P12352), PsaF (P12356), PsaH (P13352), PsaK (P14225), PsaN (Q9SBN5), Lhca3 (Q9SY97), and Lhca5 (Q9C639). Other accession numbers are reported in Table 1 and Supplemental Tables S2 and S3.

Supplemental Data

The following supplemental materials are available.

Supplemental Figure S1. Photosynthetic growth of UWO 241 under low and high salinity.

- Supplemental Figure S2. Representative traces of P700 photooxidation kinetics.
- **Supplemental Figure S3.** Photosynthetic properties of UWO 241 under various light intensities.
- Supplemental Figure S4. PSI and PSII energy partitioning in cultures of UWO 241 under LS versus HS conditions.
- Supplemental Figure S5. Maximum likelihood tree of all Lhca protein homologs identified in the UWO 241 transcriptome from HS-grown cultures.
- Supplemental Figure S6. Functional categories of proteins up-regulated and down-regulated under high salinity in UWO 241.
- Supplemental Figure S7. Heat map showing the relative changes in primary metabolite abundances in UWO 241 cultures grown under HS or LS conditions.
- Supplemental Figure S8. Cellular ATP content in UWO 241 grown under low-salinity (UWO 241-LS) versus high-salinity (UWO 241-HS) growth conditions.
- Supplemental Figure S9. Starch content of UWO 241 under LS and HS conditions.
- Supplemental Table S1. Composition of PSI and LHCI subunits in UWO 241.
- Supplemental Table S2. Down-regulated proteins in UWO 241-HS.
- Supplemental Table S3. Up-regulated proteins in UWO 241-HS.
- Supplemental Table S4. All positively identified primary metabolites in UWO 241.
- Supplemental Table S5. Metabolites present in higher abundance in UWO 241-HS
- Supplemental Table S6. Metabolites present in lower abundance in UWO 241-HS

ACKNOWLEDGMENTS

We thank the staff (Dr. Andor Kiss and Xiaoyun Deng) of the Center for Bioinformatics and Functional Genomics at Miami University for instrumentation and computational support. We also thank people from the Kramer Laboratory (Drs. David Kramer, Jeffrey Cruz, Robert Zegarac, and Ben Lucker) for their suggestions to set up and optimize the IDEAspec for spectroscopic measurements in UWO 241. We thank the staff at the West Coast Metabolomics Center for performing the metabolite extraction and identification.

Received October 17, 2019; accepted March 8, 2020; published March 30, 2020.

LITERATURE CITED

- Baker NR (2008) Chlorophyll fluorescence: A probe of photosynthesis in vivo. Annu Rev Plant Biol 59: 89–113
- Baker NR, Harbinson J, Kramer DM (2007) Determining the limitations and regulation of photosynthetic energy transduction in leaves. Plant Cell Environ 30: 1107–1125
- Carrillo LR, Froehlich JE, Cruz JA, Savage LJ, Kramer DM (2016) Multilevel regulation of the chloroplast ATP synthase: The chloroplast NADPH thioredoxin reductase C (NTRC) is required for redox modulation specifically under low irradiance. Plant J 87: 654–663
- Carvalho PC, Fischer JS, Chen EI, Yates JR III, Barbosa VC (2008) PatternLab for proteomics: A tool for differential shotgun proteomics. BMC Bioinformatics 9: 316
- Chaux F, Johnson X, Auroy P, Beyly-Adriano A, Te I, Cuiné S, Peltier G (2017) PGRL1 and LHCSR3 compensate for each other in controlling photosynthesis and avoiding photosystem I photoinhibition during high light acclimation of *Chlamydomonas* cells. Mol Plant 10: 216–218
- Chong J, Soufan O, Li C, Caraus I, Li S, Bourque G, Wishart DS, Xia J (2018) MetaboAnalyst 4.0: Towards more transparent and integrative metabolomics analysis. Nucleic Acids Res 46: W486–W494

- Cook G, Teufel A, Kalra I, Li W, Wang X, Priscu J, Morgan-Kiss R (2019)
 The Antarctic psychrophiles *Chlamydomonas* spp. UWO241 and ICE-MDV exhibit differential restructuring of photosystem I in response to iron. Photosynth Res 141: 209–228
- Cvetkovska M, Hüner NP, Smith DR (2017) Chilling out: The evolution and diversification of psychrophilic algae with a focus on Chlamydomonadales. Polar Biol 40: 1169–1184
- Cvetkovska M, Szyszka-Mroz B, Possmayer M, Pittock P, Lajoie G, Smith DR, Hüner NPA (2018) Characterization of photosynthetic ferredoxin from the Antarctic alga *Chlamydomonas* sp. UWO241 reveals novel features of cold adaptation. New Phytol 219: 588–604
- DalCorso G, Pesaresi P, Masiero S, Aseeva E, Schünemann D, Finazzi G, Joliot P, Barbato R, Leister D (2008) A complex containing PGRL1 and PGR5 is involved in the switch between linear and cyclic electron flow in Arabidopsis. Cell 132: 273–285
- Dolhi JM, Maxwell DP, Morgan-Kiss RM (2013) The Antarctic Chlamy-domonas raudensis: An emerging model for cold adaptation of photosynthesis. Extremophiles 17: 711–722
- Driever SM, Simkin AJ, Alotaibi S, Fisk SJ, Madgwick PJ, Sparks CA, Jones HD, Lawson T, Parry MAJ, Raines CA (2017) Increased SBPase activity improves photosynthesis and grain yield in wheat grown in greenhouse conditions. Philos Trans R Soc Lond B Biol Sci 372: 20160384
- Dumas L, Chazaux M, Peltier G, Johnson X, Alric J (2016) Cytochrome b₆f function and localization, phosphorylation state of thylakoid membrane proteins and consequences on cyclic electron flow. Photosynth Res 129: 307–320
- Ensminger I, Busch F, Huner NPA (2006) Photostasis and cold acclimation: Sensing low temperature through photosynthesis. Physiol Plant 126: 28–44
- Fiehn O, Wohlgemuth G, Scholz M (2005) Setup and annotation of metabolomic experiments by integrating biological and mass spectrometric metadata. In B Ludäscher, and L Raschid, eds, Data Integration in the Life Sciences. Springer, Berlin, pp 224–239
- Fiehn O, Wohlgemuth G, Scholz M, Kind T, Lee DY, Lu Y, Moon S, Nikolau B (2008) Quality control for plant metabolomics: Reporting MSI-compliant studies. Plant J 53: 691–704
- Florez-Sarasa I, Noguchi K, Araújo WL, Garcia-Nogales A, Fernie AR, Flexas J, Ribas-Carbo M (2016) Impaired cyclic electron flow around photosystem I disturbs high-light respiratory metabolism. Plant Physiol 172: 2176–2189
- He Y, Fu J, Yu C, Wang X, Jiang Q, Hong J, Lu K, Xue G, Yan C, James A, et al (2015) Increasing cyclic electron flow is related to Na⁺ sequestration into vacuoles for salt tolerance in soybean. J Exp Bot 66: 6877–6889
- Horváth EM, Peter SO, Joët T, Rumeau D, Cournac L, Horváth GV, Kavanagh TA, Schäfer C, Peltier G, Medgyesy P (2000) Targeted inactivation of the plastid *ndhB* gene in tobacco results in an enhanced sensitivity of photosynthesis to moderate stomatal closure. Plant Physiol 123: 1337–1350
- **Huang W, Yang SJ, Zhang SB, Zhang JL, Cao KF** (2012) Cyclic electron flow plays an important role in photoprotection for the resurrection plant *Paraboea rufescens* under drought stress. Planta **235**: 819–828
- Huang W, Zhang SB, Xu JC, Liu T (2017) Plasticity in roles of cyclic electron flow around photosystem I at contrasting temperatures in the chilling-sensitive plant Calotropis gigantea. Environ Exp Bot 141: 145–153
- Hüner NPA, Dahal K, Bode R, Kurepin LV, Ivanov AG (2016) Photosynthetic acclimation, vernalization, crop productivity and 'the grand design of photosynthesis.'. J Plant Physiol 203: 29–43
- Hüner NPA, Öquist G, Melis A (2003) Photostasis in plants, green algae and cyanobacteria: The role of light harvesting antenna complexes. In BR Green, and WW Parson, eds, Advances in Photosynthesis and Respiration Light Harvesting Antennas in Photosynthesis, Vol Vol 13. Kluwer Academic Publishers, Dordrecht, The Netherlands, pp 401–421
- Hüner NPA, Öquist G, Sarhan F (1998) Energy balance and acclimation to light and cold. Trends Plant Sci 3: 224–230
- Ishikawa N, Takabayashi A, Noguchi K, Tazoe Y, Yamamoto H, von Caemmerer S, Sato F, Endo T (2016) NDH-mediated cyclic electron flow around photosystem I is crucial for C4 photosynthesis. Plant Cell Physiol 57: 2020–2028
- Ivanov AG, Morgan RM, Gray GR, Velitchkova MY, Huner NP (1998)
 Temperature/light dependent development of selective resistance to photoinhibition of photosystem I. FEBS Lett 430: 288–292

- Iwai M, Takizawa K, Tokutsu R, Okamuro A, Takahashi Y, Minagawa J (2010) Isolation of the elusive supercomplex that drives cyclic electron flow in photosynthesis. Nature 464: 1210–1213
- Jeong J, Baek K, Kirst H, Melis A, Jin E (2017) Loss of CpSRP54 function leads to a truncated light-harvesting antenna size in *Chlamydomonas* reinhardtii. Biochim Biophys Acta Bioenerg 1858: 45–55
- Joliot P, Johnson GN (2011) Regulation of cyclic and linear electron flow in higher plants. Proc Natl Acad Sci USA 108: 13317–13322
- Kanazawa A, Kramer DM (2002) In vivo modulation of nonphotochemical exciton quenching (NPQ) by regulation of the chloroplast ATP synthase. Proc Natl Acad Sci USA 99: 12789–12794
- Kind T, Wohlgemuth G, Lee DY, Lu Y, Palazoglu M, Shahbaz S, Fiehn O (2009) FiehnLib: Mass spectral and retention index libraries for metabolomics based on quadrupole and time-of-flight gas chromatography/ mass spectrometry. Anal Chem 81: 10038–10048
- Kramer DM, Cruz JA, Kanazawa A (2003) Balancing the central roles of the thylakoid proton gradient. Trends Plant Sci 8: 27–32
- Kramer DM, Evans JR (2011) The importance of energy balance in improving photosynthetic productivity. Plant Physiol 155: 70–78
- Krause GH, Weis E (1991) Chlorophyll fluorescence and photosynthesis: The basics. Annu Rev Plant Physiol Plant Mol Biol 42: 313–349
- Laemmli UK (1970) Cleavage of structural proteins during the assembly of the head of bacteriophage T4. Nature 227: 680–685
- Lefebvre S, Lawson T, Zakhleniuk OV, Lloyd JC, Raines CA, Fryer M (2005) Increased sedoheptulose-1,7-bisphosphatase activity in transgenic tobacco plants stimulates photosynthesis and growth from an early stage in development. Plant Physiol 138: 451–460
- Li L, Aro EM, Millar AH (2018) Mechanisms of photodamage and protein turnover in photoinhibition. Trends Plant Sci 23: 667–676
- Livingston AK, Cruz JA, Kohzuma K, Dhingra A, Kramer DM (2010) An Arabidopsis mutant with high cyclic electron flow around photosystem I (hcef) involving the NADPH dehydrogenase complex. Plant Cell 22: 221–233
- Lucker B, Kramer DM (2013) Regulation of cyclic electron flow in Chlamydomonas reinhardtii under fluctuating carbon availability. Photosynth Res 117: 449–459
- Maeda H, Dudareva N (2012) The shikimate pathway and aromatic amino acid biosynthesis in plants. Annu Rev Plant Biol 63: 73–105
- Magnuson A, Cardona T (2016) Thylakoid membrane function in heterocysts. Biochim Biophys Acta 1857: 309–319
- Magnuson A, Krassen H, Stensjö K, Ho FM, Styring S (2011) Modeling photosystem I with the alternative reaction center protein PsaB2 in the nitrogen fixing cyanobacterium *Nostoc punctiforme*. Biochim Biophys Acta 1807: 1152–1161
- Minagawa J (2016) A supercomplex of cytochrome bf and photosystem I for cyclic electron flow. In W Cramer, and T Kallas, eds, Cytochrome Complexes: Evolution, Structures, Energy Transduction, and Signaling. Springer, Dordrecht, The Netherlands, pp 453–462
- Morgan RM, Ivanov AG, Priscu JC, Maxwell DP, Hüner NPA (1998) Structure and composition of the photochemical apparatus of the Antarctic green alga, Chlamydomonas subcaudata. Photosynth Res 56: 303–314
- Morgan-Kiss R, Ivanov AG, Williams J, Khan M, Hüner NP (2002a) Differential thermal effects on the energy distribution between photosystem II and photosystem I in thylakoid membranes of a psychrophilic and a mesophilic alga. Biochim Biophys Acta 1561: 251–265
- Morgan-Kiss RM, Ivanov AG, Hüner NPA (2002b) The Antarctic psychrophile, Chlamydomonas subcaudata, is deficient in state I-state II transitions. Planta 214: 435–445
- Morgan-Kiss RM, Ivanov AG, Modla S, Czymmek K, Hüner NPA, Priscu JC, Lisle JT, Hanson TE (2008) Identity and physiology of a new psychrophilic eukaryotic green alga, Chlorella sp., strain BI, isolated from a transitory pond near Bratina Island, Antarctica. Extremophiles 12: 701–711
- Morgan-Kiss RM, Ivanov AG, Pocock T, Król M, Gudynaite-Savitch L, Hüner NPA (2005) The Antarctic psychrophile, Chlamydomonas raudensis Ettl (UWO 241) (Chlorophyceae, Chlorophyta) exhibits a limited capacity to photoacclimate to red light. J Phycol 41: 791–800
- Morgan-Kiss RM, Priscu JC, Pocock T, Gudynaite-Savitch L, Huner NP (2006) Adaptation and acclimation of photosynthetic microorganisms to permanently cold environments. Microbiol Mol Biol Rev 70: 222–252
- Munekage Y, Hashimoto M, Miyake C, Tomizawa K, Endo T, Tasaka M, Shikanai T (2004) Cyclic electron flow around photosystem I is essential for photosynthesis. Nature **429**: 579–582

- Munekage YN, Genty B, Peltier G (2008) Effect of PGR5 impairment on photosynthesis and growth in *Arabidopsis thaliana*. Plant Cell Physiol 49: 1688–1698
- Murthy HN, Lee EJ, Paek KY (2014) Production of secondary metabolites from cell and organ cultures: Strategies and approaches for biomass improvement and metabolite accumulation. Plant Cell Tissue Organ Cult 118: 1–16
- Nawrocki W, Bailleul B, Picot D, Cardol P, Rappaport F, Wollman FA, Joliot P (2019) The mechanism of cyclic electron flow. Biochim Biophys Acta Bioenerg 1860: 433–438
- Neale PJ, Priscu JC (1990) Structure and function of the photochemical apparatus in the phytoplankton of ice-covered Lake Bonney. Antarct J US 25: 225
- Neale PJ, Priscu JC (1995) The photosynthetic apparatus of phytoplankton from a perennially ice-covered Antarctic lake: Acclimation to an extreme shade environment. Plant Cell Physiol 36: 253–263
- Pocock T, Vetterli A, Falk S (2011) Evidence for phenotypic plasticity in the Antarctic extremophile *Chlamydomonas raudensis* Ettl. UWO 241. J Exp Bot 62: 1169–1177
- Possmayer M, Berardi G, Beall BFN, Trick CG, Hüner NPA, Maxwell DP (2011) Plasticity of the psychrophilic green alga *Chlamydomonas raudensis* (UWO 241) (Chlorophyta) to supraoptimal temperature stress. J Phycol 47: 1098–1109
- Priscu JC, Wolf CF, Takacs CD, Fritsen CH, Laybourn-Parry J, Roberts JKM, Berry-Lyons W (1999) Carbon transformations in the water column of a perennially ice-covered Antarctic lake. Bioscience **49:** 997–1008
- Raymond JA, Janech MG, Fritsen CH (2009) Novel ice-binding proteins from a psychrophilic Antarctic alga (Chlamydomonadaceae, Chlorophyceae). J Phycol 45: 130–136
- Sacksteder CA, Kramer DM (2000) Dark-interval relaxation kinetics (DIRK) of absorbance changes as a quantitative probe of steady-state electron transfer. Photosynth Res 66: 145–158
- Shimakawa G, Shaku K, Miyake C (2016) Oxidation of P700 in photosystem I is essential for the growth of cyanobacteria. Plant Physiol 172: 1443–1450
- Siaut M, Cuiné S, Cagnon C, Fessler B, Nguyen M, Carrier P, Beyly A, Beisson F, Triantaphylidès C, Li-Beisson Y, et al (2011) Oil accumulation in the model green alga *Chlamydomonas reinhardtii:* Characterization, variability between common laboratory strains and relationship with starch reserves. BMC Biotechnol 11: 7
- Steinbeck J, Ross IL, Rothnagel R, Gäbelein P, Schulze S, Giles N, Ali R, Drysdale R, Sierecki E, Gambin Y, et al (2018) Structure of a PSI-LHCI-cyt b₆f supercomplex in *Chlamydomonas reinhardtii* promoting cyclic electron flow under anaerobic conditions. Proc Natl Acad Sci USA 115: 10517–10522
- Strand DD, Livingston AK, Satoh-Cruz M, Froehlich JE, Maurino VG, Kramer DM (2015) Activation of cyclic electron flow by hydrogen peroxide in vivo. Proc Natl Acad Sci USA 112: 5539–5544
- Suorsa M (2015) Cyclic electron flow provides acclimatory plasticity for the photosynthetic machinery under various environmental conditions and developmental stages. Front Plant Sci 6: 800
- Szyszka B, Ivanov AG, Hüner NPA (2007) Psychrophily is associated with differential energy partitioning, photosystem stoichiometry and polypeptide phosphorylation in Chlamydomonas raudensis. Biochim Biophys Acta 1767: 789–800
- Szyszka-Mroz B, Cvetkovska M, Smith DR, Possmayer M, Maxwell DP, Hüner NPA (2019) Cold-adapted protein kinases and thylakoid remodeling impact energy distribution in an Antarctic psychrophile. Plant Physiol 180: 1291–1309
- Szyszka-Mroz B, Pittock P, Ivanov AG, Lajoie G, Hüner NP (2015) The Antarctic psychrophile, *Chlamydomonas* sp. UWO 241 preferentially phosphorylates a photosystem I-cytochrome b6/f supercomplex. Plant Physiol 169: 717–736
- Takabayashi A, Kishine M, Asada K, Endo T, Sato F (2005) Differential use of two cyclic electron flows around photosystem I for driving CO₂-concentration mechanism in C4 photosynthesis. Proc Natl Acad Sci USA **102:** 16898–16903
- Takahashi H, Clowez S, Wollman FA, Vallon O, Rappaport F (2013) Cyclic electron flow is redox-controlled but independent of state transition. Nat Commun 4: 1954
- Tamoi M, Nagaoka M, Miyagawa Y, Shigeoka S (2006) Contribution of fructose-1,6-bisphosphatase and sedoheptulose-1,7-bisphosphatase to

- the photosynthetic rate and carbon flow in the Calvin cycle in transgenic plants. Plant Cell Physiol 47:380-390
- Terashima M, Petroutsos D, Hüdig M, Tolstygina I, Trompelt K, Gäbelein P, Fufezan C, Kudla J, Weinl S, Finazzi G, et al (2012) Calcium-dependent regulation of cyclic photosynthetic electron transfer by a CAS, ANR1, and PGRL1 complex. Proc Natl Acad Sci USA 109: 17717–17722
- Thalmann M, Pazmino D, Seung D, Horrer D, Nigro A, Meier T, Kölling K, Pfeifhofer HW, Zeeman SC, Santelia D (2016) Regulation of leaf starch degradation by abscisic acid is important for osmotic stress tolerance in plants. Plant Cell 28: 1860–1878
- Tohge T, Watanabe M, Hoefgen R, Fernie AR (2013) Shikimate and phenylalanine biosynthesis in the green lineage. Front Plant Sci 4: 62
- Tzin V, Galili G (2010) The biosynthetic pathways for shikimate and aromatic amino acids in *Arabidopsis thaliana*. The Arabidopsis Book 8: e0132, doi: 10.1199/tab.0132
- Valledor L, Weckwerth W (2014) An improved detergent-compatible gelfractionation LC-LTQ-Orbitrap-MS workflow for plant and microbial proteomics. In J Jorrin-Novo, S Komatsu, W Weckwerth, and S Wienkoop, eds, Plant Proteomics. Humana Press, Totowa, NJ, pp 347–358
- van den Berg RA, Hoefsloot HC, Westerhuis JA, Smilde AK, van der Werf MJ (2006) Centering, scaling, and transformations: Improving

- the biological information content of metabolomics data. BMC Genomics 7:142
- Wang X, Chang L, Wang B, Wang D, Li P, Wang L, Yi X, Huang Q, Peng M, Guo A (2013) Comparative proteomics of *Thellungiella halophila* leaves from plants subjected to salinity reveals the importance of chloroplastic starch and soluble sugars in halophyte salt tolerance. Mol Cell Proteomics 12: 2174–2195
- Wang X, Liu W, Xin C, Zheng Y, Cheng Y, Sun S, Li R, Zhu XG, Dai SY, Rentzepis PM, et al (2016) Enhanced limonene production in cyanobacteria reveals photosynthesis limitations. Proc Natl Acad Sci USA 113: 14225–14230
- Xu T, Venable J, Park SK, Cociorva D, Lu B, Liao L, Wohlschlegel J, Hewel J, Yates J III (2006) ProLuCID, a fast and sensitive tandem mass spectra-based protein identification program. Mol Cell Proteom 5: S174
- Yamori W, Makino A, Shikanai T (2016) A physiological role of cyclic electron transport around photosystem I in sustaining photosynthesis under fluctuating light in rice. Sci Rep 6: 20147
- Zhang R, Cruz JA, Kramer DM, Magallanes-Lundback ME, Dellapenna D, Sharkey TD (2009) Moderate heat stress reduces the pH component of the transthylakoid proton motive force in light-adapted, intact to-bacco leaves. Plant Cell Environ 32: 1538–1547